Chapter 2
Unexpected Excessive Settlements: Kansai International Airport, Japan

TABLE OF CONTENTS

A.M. Puzrin et al., *Geomechanics of Failures*, DOI 10.1007/978-90-481-3531-8_2,

Chapter 2

Unexpected Excessive Settlements: Kansai International Airport, Japan

2.1 Case Description

2.1.1 Introduction

Kansai International Airport (KIA) in Osaka Bay, Japan (Fig. 2.1a) was singled out by the American Society of Civil Engineers as one of the "Monuments of the Millennium" – a designation awarded to the ten civil engineering projects deemed to have had the greatest positive impact on life in the 20th century. This is an even more remarkable achievement, considering that the first phase of the airport construction experienced some problems which, in a broader sense, could be characterized as a geotechnical failure. Built on a 1.25 km × 4 km man-made island (Fig. 2.1b), 5 km offshore at an average water depth of 18 m, this first phase experienced unexpected excessive settlements. These settlements were not correctly predicted either before or during the construction and caused delays, considerably increasing the cost of the 14 billion dollar project.

(a) (b)

Figure 2.1 Kansai International Airport (Google Earth ©): (a) Osaka Bay; (b) the islands of Phase I and Phase II.

2.1.2 Construction

Construction of the first phase island of Kansai International Airport started in January 1987 and finished in December 1991. Construction of the airport facilities followed and the airport began operations in September 1994. In the five years of the island's construction, more than 180 million m^3 of granular fill with a height of about 33 m were placed on the seabed, which consists of more than 1,200 m of sediments (Fig. 2.2). Only the upper 160 m, however, are considered to be

compressible: the top 20 m are soft alluvial Holocene clays (Ma13), followed by the alternation of sand and clay layers of Pleistocene origin (Ma 7 – 12, "Ma" stands for marine clay).

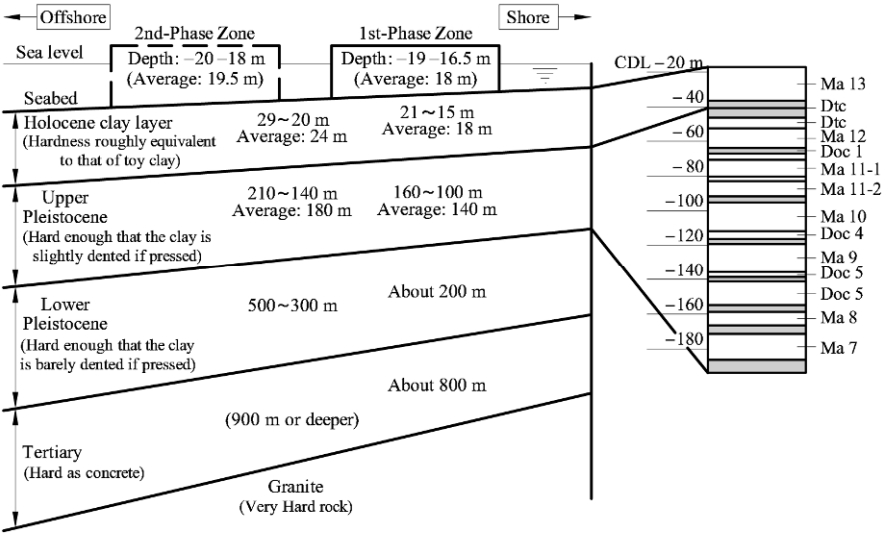

Figure 2.2 The soil profile of the seabed (after Akai *et al*., 1995; Akai and Tanaka, 1999: © 1999 Taylor and Francis Group. Used with permission; KALD, 2009): dark layers-sand, white-marine clays Ma7 ─ Ma13.

The construction process included the following stages. First, the top 20 m of the seabed (Holocene clays) were treated within the design island area by installing vertical sand drains to accelerate compaction under the backfill. Next, the perimeter seawalls were built (Fig. 2.3). Subsequently, the land reclamation took place, in which the granular fill, taken from a number of excavations in the Osaka area (they practically levelled a couple of large hills), was placed within the seawalls up to a depth of about 3 m below the water level using bottom-dump barges. The final step was accomplished by means of four large barges, anchored inside the seawalls, which transferred the fill brought by the smaller barges from across the bay, to bring the island to the required 4 m above the water level. This height is to guarantee that the airport will not be swamped by high tides brought by typhoons that hit the coast of Japan every September.

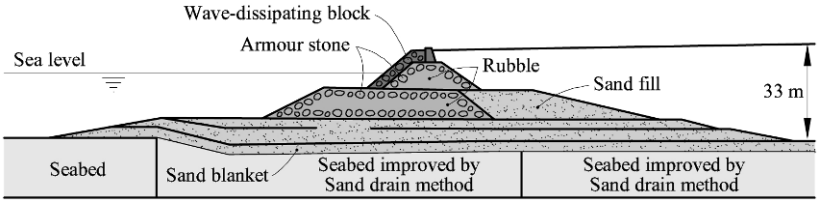

Figure 2.3 The cross-section of a seawall (after KALD, 2009).

Two important notes on the construction process: (1) no measures have been taken to accelerate the consolidation settlements in the lower (Pleistocene) clay strata, due to its considerable depth (instead, a special effort was made to predict the settlements as accurate as possible); (2) once the final step was complete, there was no way to add the fill on top of the island using the same method. The problem was that the barges could not enter the island's interior anymore. Combination of these two factors shows that the planning and design processes did not allow for the risk of extra settlement due to consolidation of the Pleistocene clay strata. No construction process was devised which could cope with these settlements.

2.1.3 The history of settlements

Thanks to the vertical drains, the top 20 m of the Holocene clay reached almost 90% of its final 6 m settlement during the construction (Handy, 2002). These settlements were accounted for in the design, being compensated by an additional 6 m thick layer of fill and additional height of the seawalls. What was apparently not fully accounted for were the excessive settlements of the Pleistocene clays and their slow accumulation in time (Fig. 2.4). By 1999, immediate settlements of about 1 m magnitude were recorded followed by additional 5 m of settlement and continue to increase at a rate of about 15 cm per year. Adding extra layers of fill during the construction compensated only for immediate settlements and a small part of the consolidation settlement of the Pleistocene sediments.

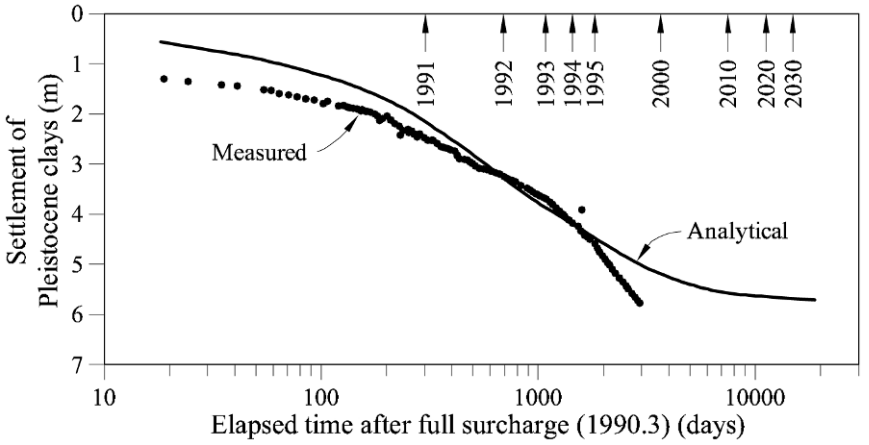

Figure 2.4 Settlements of the island (at point A in Fig. 2.1b) due to consolidation of Pleistocene clays (after Endo *et al*., 1991; Akai and Tanaka, 1999: © 1999 Taylor and Francis Group. Used with permission).

The original design did not anticipate these developments. As soon as it was clear that the Pleistocene clays were the source of these excessive settlements, attempts were made to re-evaluate them as shown in Figure 2.4 (Endo *et al*., 1991). These attempts were based on field measurements at the beginning of the

construction and failed to provide a reasonably accurate prediction. They were continuously corrected, but each time a prediction was made, the island provided a new "surprise". First, it was a sizeable immediate settlement. Next, it was a much slower than expected rate of settlement at the beginning of the consolidation. Finally, these settlements did not seem to slow down as much as expected towards the end of the consolidation.

2.1.4 The problem

Many different factors affected the settlement prediction of the Kansai International Airport. This chapter will focus on just three of them, mentioned above: the immediate settlement, the slower settlement rate in the beginning, and the faster rate towards the end of consolidation of the upper Pleistocene clays.

Immediate settlements are caused by the three-dimensionality of the real problem, as compared to the one dimensional consolidation theory, in particular, by non-negligible lateral strains. They are also affected by the compressibility of sand layers where dissipation of pore water pressures takes place very quickly.

The rate of consolidation is determined to a large extent by the length of the drainage path. Conventionally, a sand layer between two clay layers is considered to work as a drain. In the case of the Pleistocene strata, however, some of the sand layers proved to be lenses, entirely enclosed within the clay layer, which was confirmed by very slow dissipation of pore water pressures measured in the sand layers 10 years after the land reclamation (Fig. 2.5).

Finally, the consolidation process is not the only one controlling the rate of settlements in clay. Even when the excess pore water pressure has completely dissipated, the settlement continues, which is called creep or *secondary compression*. Towards the end of primary consolidation, a contribution of the secondary compression becomes more pronounced and may produce significant increases in settlements long after the primary consolidation is over.

All these factors are rather difficult to quantify accurately in advance of the construction. This is not, however, good news for designers. Is there any way to resolve this dilemma?

2.1.5 The observational method

The major problem with land reclamation projects of this scale is that it is almost impossible to provide an accurate prediction of the rates of settlement based solely on the results of site investigation and laboratory consolidation tests. There are two major reasons for that: (1) large spatial variability of soil properties and drainage geometry and (2) laboratory tests often produce the values of the coefficient of consolidation c_v and secondary compression C_α within two orders of magnitude from the field values. Therefore, such estimates can only be used as initial conditions for design.

In such a case, the design should be left flexible to accommodate changes, as construction proceeds. These changes are based on the continuous monitoring of significant field parameters and on inverse analysis of the field measurements. This back calculation allows for the model parameters to be updated using real

field data and then utilized for the next stages of analysis and design. In geotechnical engineering this approach is called *the observational method*. The purpose of this chapter is to demonstrate a simplified back-calculation procedure for the field data from the KIA.

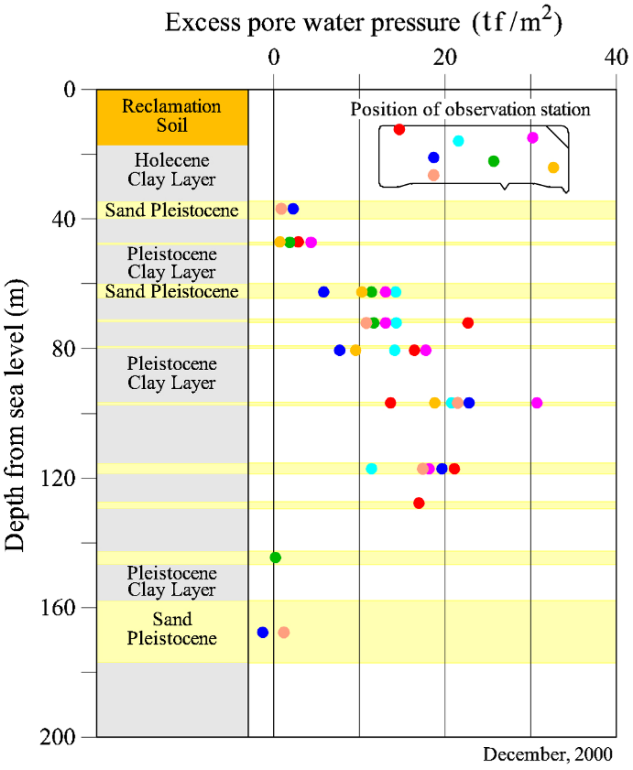

Figure 2.5 Drainage in the sand layers: 1 tf/m^2 = 9.8 kPa (after KALD, 2009).

2.2 The One-Dimensional Theory

Marine deposits near the coast and big river deltas are often layered systems due to their alluvial nature. In general, they are built of alternating sand and clay layers, whose thickness depends on the geological history. The settlements of the saturated sand and clay materials are governed by different phenomena. Settlements of saturated sand layers are normally immediate settlements, provided that they work as open drains. Settlement of saturated clay layers is a time-dependent phenomenon which is governed by the following processes:

- primary consolidation – decrease in the volume of pores due to the flow of water caused by the dissipating pore water pressure gradient;
- secondary compression – decrease in the pore volume due to creep.

The total settlement of these layered systems in a one-dimensional problem is built, therefore, out of these three distinct components:

$$\rho_T(t) = \rho_I + \rho_C(t) + \rho_S(t), \tag{2.1}$$

where ρ_I is the immediate settlement (sand);
$\rho_C(t)$ is the consolidation settlement (clay);
$\rho_S(t)$ is the creep settlement (clay).

2.2.1 Immediate settlement

Immediate settlements in saturated clay layers in a one-dimensional problem should be zero, due to the small pores and incompressibility of the pore water which cannot leave the pores immediately. In reality, however, there are always some immediate settlements caused by the three-dimensionality of the real problem, which involves non-negligible lateral strains. Because of these lateral strains, some vertical settlements also occur without any change in the total volume, as required by the incompressibility condition.

In the layered sand-clay systems, however, some immediate settlements occur, even in a one-dimensional problem. This is due to the compressibility of the sand layers, where pores are sufficiently large to allow for almost immediate dissipation of pore water pressures. These immediate settlements due to a stress increase of $\Delta\sigma$ in a thin sand sublayer of thickness H, can be calculated as

$$\rho_I = H\frac{\Delta\sigma}{M_E^{\text{sand}}} = H\frac{(1+\nu)(1-2\nu)}{E(1-\nu)}\Delta\sigma, \tag{2.2}$$

where M_E^{sand} is the one-dimensional compression modulus of sand;
E is the Young modulus of sand;
$\nu = 0.2 \div 0.3$ is the Poisson ratio of sand.

Note that for clay, this formula would produce a zero settlement due to the incompressibility condition $\nu = 0.5$.

Immediate settlements take place during construction. Therefore, though important at the design stage of land reclamation (for correct estimates of the required fill volume), they do not affect the long-term behaviour of the structure and have to be properly excluded from the analysis.

2.2.2 Settlement due to one-dimensional consolidation

Calculation of the final settlement due to consolidation has been discussed in Section 1.2 (Chapter 1). By the end of the consolidation, a total stress increase of $\Delta\sigma$ in a thin sublayer of thickness H will produce an equal effective stress increment $\Delta\sigma' = \Delta\sigma$. For normally consolidated clays, this will result in a final settlement of

$$\rho_{\text{inf}} = \frac{H}{M_E^{clay}}\Delta\sigma \quad \text{or} \quad \rho_{\text{inf}} = \frac{H}{1+e_0}C_c \log\frac{\sigma_0' + \Delta\sigma}{\sigma_0'}, \tag{2.3}$$

where σ_0' is the effective normal vertical stress;

e_0 is the in-situ void ratio before the construction;

C_c is the compression index;

M_E^{clay} is the one-dimensional compression modulus of clay.

C_c and M_E^{clay} are related as follows:

$$\frac{1}{M_E^{\text{clay}}} = \frac{C_c}{1+e_0} \frac{\log\left(\sigma_0' + \Delta\sigma'\right) - \log\left(\sigma_0'\right)}{\Delta\sigma'}. \tag{2.4}$$

The development of the consolidation settlement in time is schematically presented in Figure 2.6a. The total stress increment $\Delta\sigma$ (constant in time and uniformly distributed with depth) is first entirely taken by the pore water. This causes a pressure gradient between the clay layer and draining boundaries, producing a pore water flow towards these boundaries. In the process, the excess pore pressure $\Delta u(t)$ dissipates and more load is transferred to the soil skeleton via the effective stresses $\Delta\sigma'(t) = \Delta\sigma - \Delta u(t)$, causing its compression and settlements $\rho_C(t)$.

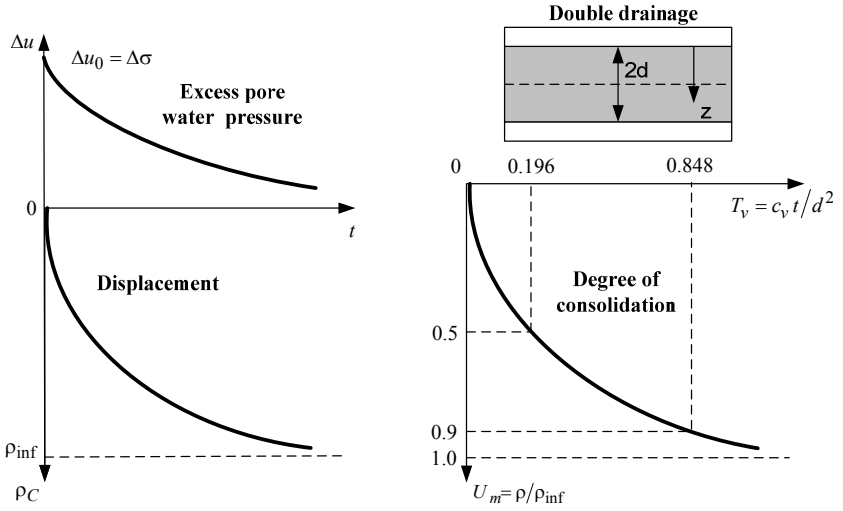

(a) (b)

Figure 2.6 One-dimensional consolidation: (a) the process; (b) analytical solution.

The analytical solution to this problem, derived by Terzaghi (1943), is presented in a non-dimensional form in Figure 2.6b:

$$U_m\left(T_v\right) = \frac{\rho_C}{\rho_{\text{inf}}} = 1 - \sum_{m=0}^{\infty} \frac{2}{M^2} \exp\left(-M^2 T_v\right), \tag{2.5}$$

where $U_m = \dfrac{\rho_C}{\rho_{\inf}}$ is the average degree of consolidation;

$T_v = \dfrac{c_v \cdot t}{d^2}$ is the non-dimensional time factor;

d is the drainage path; in a layer with double drainage, half of its thickness H;

$c_v = \dfrac{k \cdot M_E^{\text{clay}}}{\gamma_w}$ is the coefficient of consolidation;

k is the permeability coefficient;

γ_w is the unit weight of the water;

$M = \dfrac{\pi}{2}(2m+1)$, where $m = 0,\ 1,\ 2,\ ...,\ \infty$.

Relationship (2.5) can be quite accurately approximated by the following two analytical functions (Terzaghi, 1943):

$$T_v \approx \frac{\pi}{4} U_m^2, \quad \text{for } U_m \le 0.526; \tag{2.6}$$

$$T_v \approx -0.933 \cdot \log(1 - U_m) - 0.085, \quad \text{for } U_m > 0.526. \tag{2.7}$$

Using these relationships, we can describe the variation of consolidation settlement in time analytically:

$$\rho_C(t) = \rho_{\inf} \cdot U_m = \rho_{\inf} \cdot \sqrt{\frac{4 \cdot T_v}{\pi}} = \rho_{\inf} \cdot \frac{2}{d} \sqrt{\frac{c_v \cdot t}{\pi}} \quad \text{for } U_m \le 0.526; \tag{2.8}$$

$$\rho_C(t) = \rho_{\inf} \cdot U_m = \rho_{\inf} \cdot \left(1 - 10^{-\frac{c_v t / d^2 + 0.085}{0.933}} \right) \quad \text{for } U_m > 0.526. \tag{2.9}$$

For layered strata, the total settlement is calculated as the sum of the settlements of individual clay layers:

$$\rho_C(t) = \sum_{i=1}^{n} \rho_C^i(t). \tag{2.10}$$

2.2.3 Secondary compression (creep) settlements

Creep settlements begin together with the primary consolidation settlements, but become dominant only towards the end of the primary consolidation (Fig. 2.7a) and can be predicted using the formula (e.g., Mesri and Vardhanabhuti, 2005):

$$\rho_S(t) = \frac{C_\alpha}{1 + e_0} H \log\left(\frac{t}{t_p} \right), \tag{2.11}$$

where C_α is the coefficient of secondary compression;

t_p is the assumed beginning of the secondary compression, defined in Figure 2.7a at the point, where the experimental curve starts deviating from the theoretical primary consolidation line.

2.2.4 Total settlements

Using Equations (2.8) – (2.10), the variation of total settlement in time can be predicted using the following formulae:

$$\rho_T(t) = \rho_I + \rho_{\text{inf}} \frac{2}{d}\sqrt{\frac{c_v \cdot t}{\pi}} \qquad \text{for } 0 \le t \le 0.217\frac{d^2}{c_v}; \tag{2.12}$$

$$\rho_T(t) = \rho_I + \rho_{\text{inf}}\left(1 - 10^{-1.072 c_v t/d^2 - 0.091}\right) \qquad \text{for } 0.217\frac{d^2}{c_v} < t \le t_p; \tag{2.13}$$

$$\rho_T(t) = \rho_I + \rho_{\text{inf}}\left(1 - 10^{-1.072 c_v t/d^2 - 0.091}\right) + \frac{C_\alpha}{1+e_0} H \log\left(t/t_p\right) \qquad \text{for } t > t_p, \tag{2.14}$$

where ρ_I is the initial settlement;

t_p is the assumed beginning time of the secondary compression.

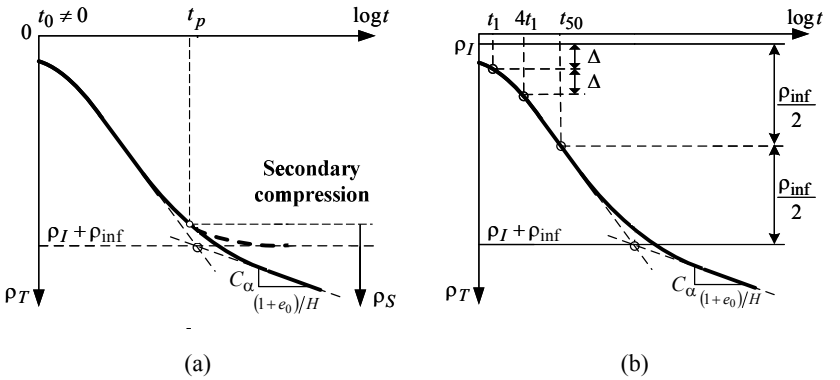

(a) (b)

Figure 2.7 Semi-logarithmic settlement-time plot: (a) secondary compression; (b) graphic procedure for back-calculation of model parameters.

2.2.5 Inverse analysis of the settlement data

The parameters in Equations (2.12) – (2.14) can be easily back-calculated from the measured settlement data using the graphic procedure in Figure 2.7b:

- Measure the settlement Δ between any two early time moments t_1 and $4t_1$, and add it to $\rho(t_1)$. Using the fact that the initial part of the settlement curve is parabolic (Eq. 2.8), this gives the initial settlement

$\rho_I = \rho(t_1) + [\rho(t_1) - \rho(4t_1)] = 2\rho(t_1) - \rho(4t_1)$;

- Draw two tangential lines to straight portions of the primary consolidation and secondary compression curves. Their intersection defines $\rho_I + \rho_{\text{inf}}$. Using ρ_I found above, this gives ρ_{inf};
- the slope of the tangent to the secondary compression curve is C_α;
- the point on the curve with $\rho(t_{50}) = \rho_I + \rho_{\text{inf}}/2$, at which the first half of the final consolidation settlement was reached ($U_m = 0.5$), gives t_{50}, so that $c_v = 0.196\, d^2/t_{50}$ (see Fig. 2.6b).

2.3 The Analysis

The one-dimensional theory presented above provides tools for a simplified analysis of the unexpected excessive settlements of Kansai International Airport.

2.3.1 Simplified model

The upper clay layer in Figure 2.8a (Holocene Clay MA13) consolidated very quickly thanks to the vertical drains and its settlement is assumed to be immediate. The nine upper Pleistocene clay layers, sandwiched between the ten sand layers (KALD, 2009) are assumed, for simplicity, to have the same thickness H = 12.0 m (Fig. 2.8b).

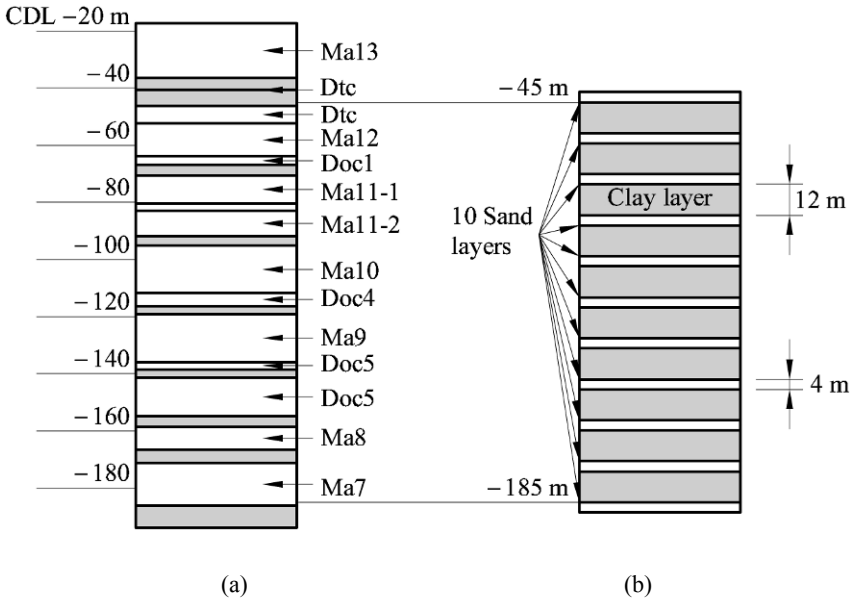

Figure 2.8 Upper Pleistocene soil profile: (a) real (after Akai and Tanaka, 1999: © 1999 Taylor and Francis Group. Used with permission); (b) simplified.

As mentioned in Section 2.1.2, as soon as it became clear that the Pleistocene clays are the source of excessive settlements, attempts were undertaken to make a prediction of their future developments. One of these predictions, by Endo *et al.* (1991), provided an analytical solution, shown in Figure 2.4 by a solid line. Our simplified model will reproduce this solution if the following assumptions are made with respect to the geometry and material properties:

- the height of the 4.0 km × 1.25 km island above the seabed is h = 33 m, out of which h_w = 29 m are below the sea level;
- the unit weights of soil are $\gamma_{\text{island}} = 21$ kN/m^3, $\gamma_{\text{seabed}} = 18$ kN/m^3;
- the overconsolidation ratio OCR of Pleistocene deposits grows linearly with depth (Akai *et al.*, 1995), therefore the lower Pleistocene clay remains overconsolidated in the process of land reclamation and can be considered incompressible;
- the Pleistocene clay is considered to be normally consolidated with consolidation parameters e_0 = 1.5, C_c = 0.6, $c_v = 1.67\times10^{-7}$ m^2/s roughly corresponding to the results of consolidation tests (Fig. 2.9);
- the upper Pleistocene clay of total thickness H = 108 m is built of nine 12 m thick sublayers interlaid by eight 4 m thick sand drains so that the average length of the vertical drainage path d = 6.0 m;
- sand layers are also present at the lower and upper boundaries of the 108 m thick Pleistocene clay layer;
- neither an initial settlement nor a settlement due to the secondary compression were considered.

2.3.2 The original prediction

In this section, using our simplified model, we reproduce the original prediction of Endo *et al.* (1991) represented by the solid curve in Figure 2.4.

The Ma13 Holocene Clay layer consolidated before the end of construction. This immediate settlement was approximately 6 m, and its increase in time is insignificant.

The final settlement due to consolidation of the Pleistocene clay layers can be calculated using formula (2.3) for each of the nine clay layers and summing their settlements:

$$\rho_{\text{inf}} = \sum_{i=1}^{i=9} \Delta\rho_{\text{inf}}^{i} = \sum_{i=1}^{i=9} \Delta H \frac{C_c}{1+e_0} \log\left(\frac{\sigma'_{0i}+\Delta\sigma}{\sigma'_{0i}}\right) = \\ = \sum_{i=1}^{i=9} 12 \frac{0.6}{1+1.5} \log\left(\frac{8D_i+403}{8D_i}\right) = 5.6 \text{ m}, \tag{2.15}$$

where $\Delta\sigma = \gamma_{\text{island}}\left(h-h_w\right)+\left(\gamma_{\text{island}}-\gamma_w\right)h_w = 21\times4+11\times29 = 403$ kPa;

$\sigma'_0 = \gamma'_{\text{seabed}} D_i = 8D_i$ is the geological stress;

$D_i = 31 \text{ m} + 16 \text{ m}\cdot\left(i-1\right)$ is the depth of the center of the i-th clay layer from the seabed surface.

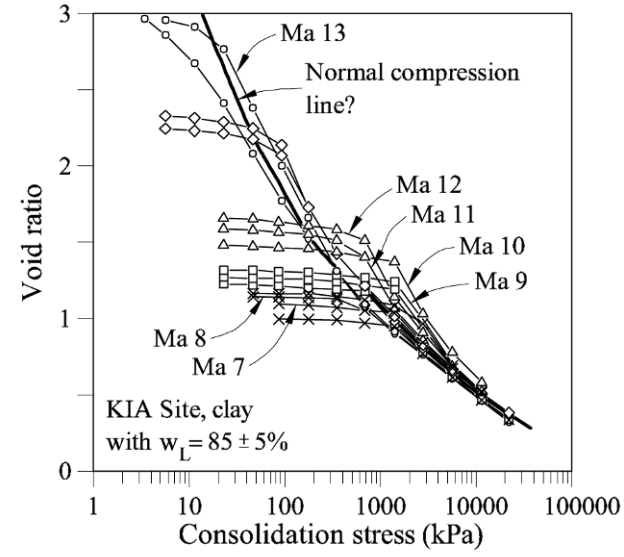

(a)

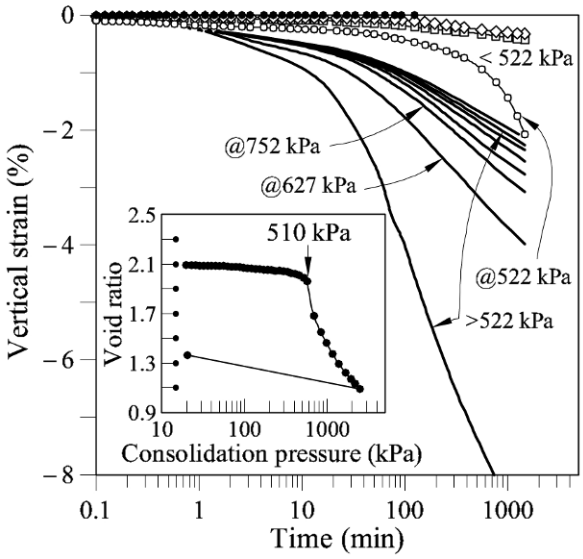

(b)

Figure 2.9 Consolidation test results for Pleistocene clays (after Akai and Tanaka, 1999: © 1999 Taylor and Francis Group. Used with permission): (a) consolidation curves; (b) settlement in time curves for M12. Here @522 kPa denotes the curve at the load close to the preconsolidation pressure of 510 kPa. Its rate of settlement is significantly higher than that of both, the overconsolidated (load < 522 kPa) and the normally consolidated (load > 522 kPa) curves, indicating destructuring, typical for aged clays.

This final 5.6 m consolidation settlement of the Pleistocene clay was also predicted by Endo *et al*. (1991) and is most likely to be a correct estimate (Akai and Tanaka, 2005). The problem of this prediction is different – it is not the value of the final consolidation settlement but the development of this settlement in time and what happens after the consolidation is over. Indeed, according to Endo *et al*. (1991), half of the Pleistocene clay settlement in all clay layers should have occurred after 490 days and 90% of it after 2,120 days, which can be also reproduced by our simplified model:

$$t_{50} = \frac{T_{v(50)} d^2}{c_v} = \frac{0.196 \times (6.0)^2}{1.67 \times 10^{-7}} \left(\frac{1}{24 \times 3600} \right) = 490 \text{ days},$$

$$t_{90} = \frac{T_{v(90)} d^2}{c_v} = \frac{0.848 \times (6.0)^2}{1.67 \times 10^{-7}} \left(\frac{1}{24 \times 3600} \right) = 2{,}120 \text{ days}.$$

In reality, however, the consolidation continued much longer. In 1999 (almost 3,200 days after the end of construction), the settlement already exceeded 6 m (the total settlement exceeded 12 m) and kept increasing at an average rate of about 15 cm per year (Fig. 2.4).

2.3.3 Correction for the initial settlement

Starting from the early stages of consolidation, it became clear that settlement of the Pleistocene deposits was much higher than expected (Fig. 2.10a). One possible reason for that could be a higher rate of consolidation, but the trend in Figure 2.10a is opposite – the rate of settlement is slower than predicted.

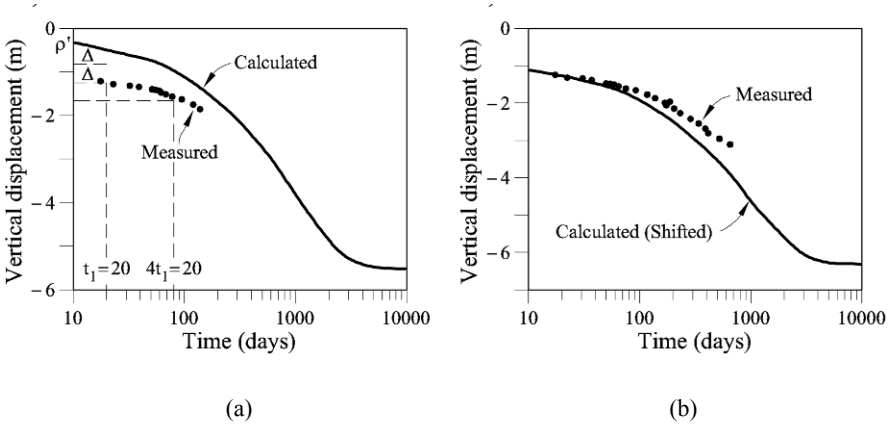

Figure 2.10 Correction for the initial settlement: (a) derivation of parameters; (b) corrected prediction.

Therefore, the most likely reason for higher settlements is an initial settlement. It can be estimated using the procedure in Figure 2.6b:

- at $t_1 = 20$ days: $\rho_{t1} = 1.25$ m;
- at $t_2 = 4t_1 = 80$ days: $\rho_{t2} = 1.60$ m;
- therefore, $\rho_I = 2\rho(t_1) - \rho(4t_1) = 2 \times 1.25 - 1.60 = 0.90$ m.

The corrected prediction (Eq. 2.12), accounting for this initial settlement $\rho_I = 0.90$ m, is shown in Figure 2.10b. While giving a good fit to the measured data up to the first 60 days, it predicts a much higher rate of consolidation later on.

2.3.4 Correction for the length of the drainage path

The rate of consolidation is governed by the consolidation coefficient c_v and the average length of the drainage path d (or, in our model, the number n of draining sand layers). Because dissipation of the excess pore water pressure in some of the sand layers was very slow (Fig. 2.5), it is most probable that the average length of the drainage path d was larger than assumed from the geometry. Also, because d in the formula for the time factor T_v is squared and c_v is not, an inaccuracy in d affects the rate of consolidation stronger.

We assume that the final settlement due to consolidation of Pleistocene clay $\rho_{inf} = 5.6$ m was correctly predicted in Equation (2.15) (see also Akai and Tanaka, 2005). Then the measured time t_{50} of the 50% of consolidation settlement (i.e. at the total settlement of $\rho_{50} = \rho_I + \rho_{inf}/2 = 3.70$ m) was 1,000 days (Fig. 2.11a) and not 490 days, as predicted by Endo *et al*. (1991).

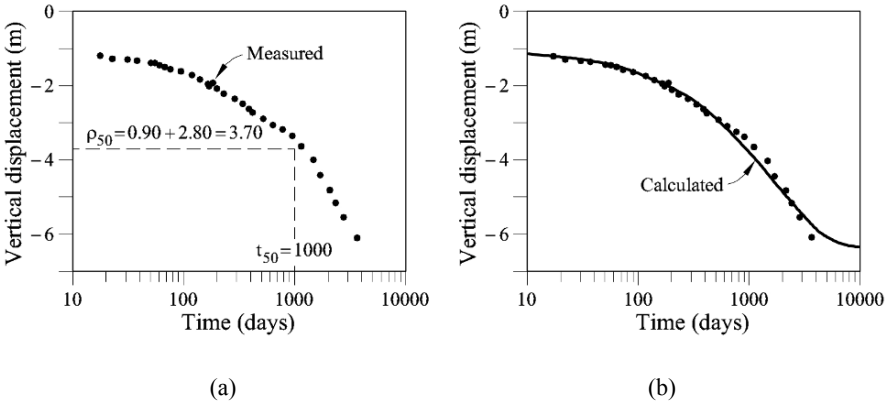

Figure 2.11 Correction for the length of the drainage path: (a) derivation of parameters; (b) corrected prediction.

The average length of the drainage path d and the number of equivalent clay layers n should be then adjusted as follows:

$$d = \sqrt{\frac{t_{50} \cdot c_v}{T_{v(50)}}} = \sqrt{\frac{1{,}000 \times 24 \times 3{,}600 \times 1.67 \times 10^{-7}}{0.196}} = 8.57 \text{ m} > 6 \text{ m}, \qquad (2.16a)$$

$$n = \frac{H}{2d} = \frac{108}{2 \times 8.57} = 6.3 < 9. \tag{2.16b}$$

The corrected prediction (using Eqs. (2.12) and (2.13)), which accounts for this modified average length of the drainage path d = 8.57 m, is shown in Figure 2.11b. While giving a good fit to the measured data up to 2,000 days, later on it predicts a lower rate of settlement.

2.3.5 Correction for the secondary compression

The most likely reason for continuing excessive settlements at the final stages of consolidation is the secondary compression. In particular, Akai and Tanaka (1999) noted a very high rate of post-consolidation settlement when effective stress slightly exceeds the pre-consolidation pressure (Fig. 2.9b, the curve @522 kPa), and related this to the phenomenon of destructuring of aged clays. In order to be able to derive parameter C_α using the procedure in Figure 2.7b, we need more data points in time. However, if the latest prediction of the consolidation curve (corrected for initial settlement and the drainage path length) were reliable, then an alternative procedure could be applied (Fig. 2.12a).

According to this procedure, t_p is taken as the moment in time when the measurements start to deviate from the theoretical consolidation line, i.e. in our case: t_p = 1,800 days. Parameter C_α is then obtained from the difference $\Delta\rho_s$ between the predicted (with $C_\alpha = 0$) and measured displacements at some time $t > t_p$, e.g., for t = 3,200 days, $\Delta\rho_s = 0.37$ m, so that

$$C_\alpha = \frac{\Delta\rho_s (1+e_0)}{H \log(t/t_p)} = \frac{0.37 \times (1+1.5)}{108 \times \log(3,200/1,800)} = 0.034\,, \quad \frac{C_\alpha}{C_c} = \frac{0.034}{0.6} = 0.057.$$

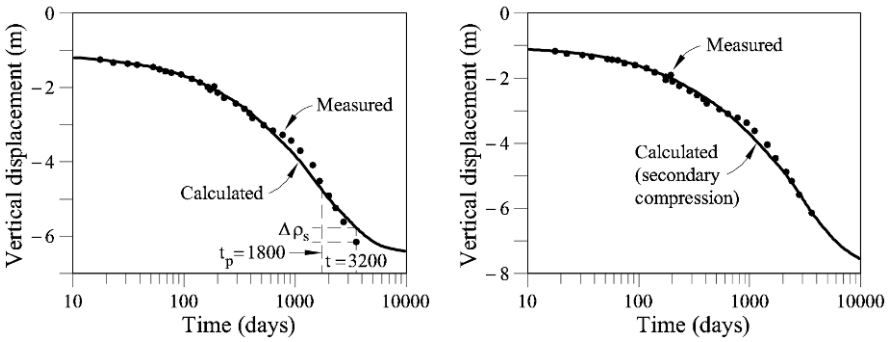

Figure 2.12 Correction for the secondary compression: (a) derivation of parameters; (b) corrected prediction.

The latter ratio of 0.057 is reasonable but somewhat high for clays, most probably due to the phenomenon of destructuring of aged clays, observed by Akai and Tanaka (1999) for the upper Pleistocene clays.

The corrected prediction (Eqs. (2.12) – (2.14)), accounting for the secondary compression with t_p = 1,800 days and $C_\alpha = 0.034$, is shown in Figure 2.12b. This prediction gives an excellent fit to the settlement data measured so far, considering the enormous simplifications which were introduced into the model.

2.3.6 Total predicted displacement

Assuming 50 years for the airport lifetime, we obtain the creep settlement:

$$\rho_S = \frac{C_\alpha}{1+e_0} H \log\left(\frac{t}{t_p}\right) = \frac{0.034}{1+1.5} \times 108 \times \log\left(\frac{50\times 365}{1,800}\right) = 1.5 \text{ m.}$$

The total predicted displacement (after 50 years) for the Pleistocene layer then becomes:

$$\rho_T^{Pl} = \rho_I + \rho_{\text{inf}} + \rho_S = 0.9 + 5.6 + 1.5 = 8.0 \text{ m.}$$

Adding the settlement of the Holocene clay layer, we obtain (Fig. 2.13):

$$\rho_T = 8.0 + 6.0 = 14.0 \text{ m.}$$

The latest prediction of the 50 years settlement (Akai and Tanaka, 2005) is 14.3 m. If the design of the island was produced using the originally predicted 11.6 m settlement, the planned 4 m embankment over the sea level would, over the years, become reduced to just 1.6 m. This would not be sufficient to withstand the high tides brought by typhoons.

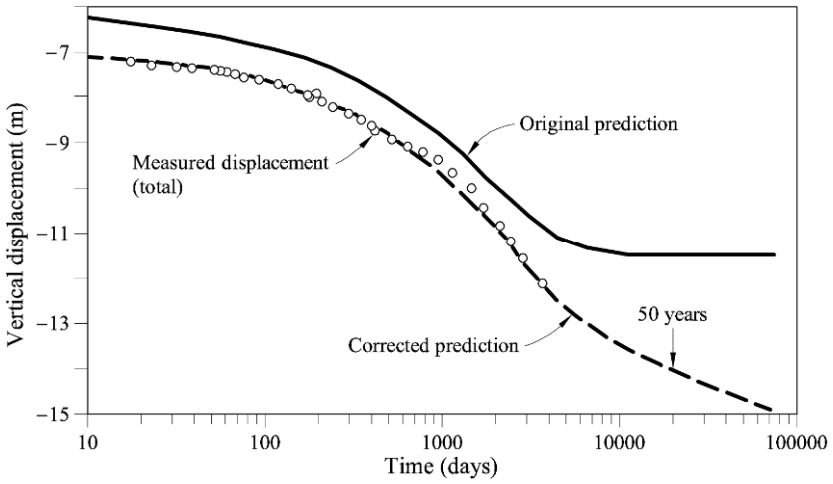

Figure 2.13 Comparison between the original and updated predictions of the total settlement.

2.3.7 Discussion

The simplified geotechnical model of the Kansai International Airport settlement is one-dimensional and therefore cannot account for the spatial variability of geometry, loading and soil properties, as well as for the three-dimensional effects of stress and strain distribution. It also focused only on the following phenomena: initial settlements, drainage and creep. The overconsolidated behaviour and complex compression characteristics of aged clays were not considered. Nevertheless, the model managed to produce a remarkably good fit to the measured settlements. Furthermore, its prediction of future settlements is consistent with those produced by more sophisticated models. This became possible because the model parameters were back-calculated using the field data. This example demonstrates the importance of simple geotechnical inverse analysis in understanding and predicting the settlements in large-scale land reclamation problems.

2.4 Mitigation Measures

Mitigation of damage due to global excessive settlements in land reclamation is a difficult task. The addition of a fill to compensate for these settlements after an island is complete is often not feasible technologically (e.g., the barges cannot reach the inside of the island) or due to operational reasons (it is unthinkable to shut down an airport). In addition, this fill, due to its weight, would probably cause additional settlements. Therefore, the negative effects of the settlements of the island on its ability to withstand high tides should be mitigated by extending the height of the seawalls accompanied by their reinforcement.

The major sources of worry, however, are the differential settlements affecting the structures. The passenger terminal building (Fig. 2.14a) is a structure with a key service floor area of 0.3 km^2. It consists of a 4 (3 + 1 basement) stories main building (320×150 m) and two 3 stories wing buildings (670×40 m each). These buildings are supported by 874 columns over their total length of 1,660 m.

The major problem with the main building is that, because of the basement, its weight represents only half of the weight of the soil it displaced. Therefore, to ensure that the island and the structure sank at the same speed rate, the basement of the terminal was lined with a quarter of a million tons of iron ore. As is seen in Figure 2.14b, this measure had only limited success – the solid line shows that the ground under the main building sank by October 2003 considerably less than the ground under the wing buildings. Most probably, the weight compensation was only partial.

In order to compensate for continuing differential settlements during the operation of the building, the supporting columns have been supplied with a jack-up system allowing for the adjustment of their heights. These adjustments have been performed two or three times a year by jack-ups and inserting thin plates (Matsui *et al.*, 2003) to keep the differential settlements within the design limits: $\theta = 1/400$ for local distortion angle of the roof structure of the main frame and $\theta = 1/600$ for the roof structure of the wings. The dashed line in Figure 2.14b indicates the level of the columns corrected by the jack-ups. As is seen, in spite of

the fact that by October 2003 the maximum correction height has reached for some columns almost 60 cm, the differential settlement criteria had not been yet satisfied. The maximum differential settlement between the center of the main building and the lowest columns of the south wing building was 95 cm, resulting in the maximum inclination of the dashed line of $\theta = 1/450$, which exceeds by far the design limit of $\theta = 1/600$ for local distortion angle of the roof structure of the wings.

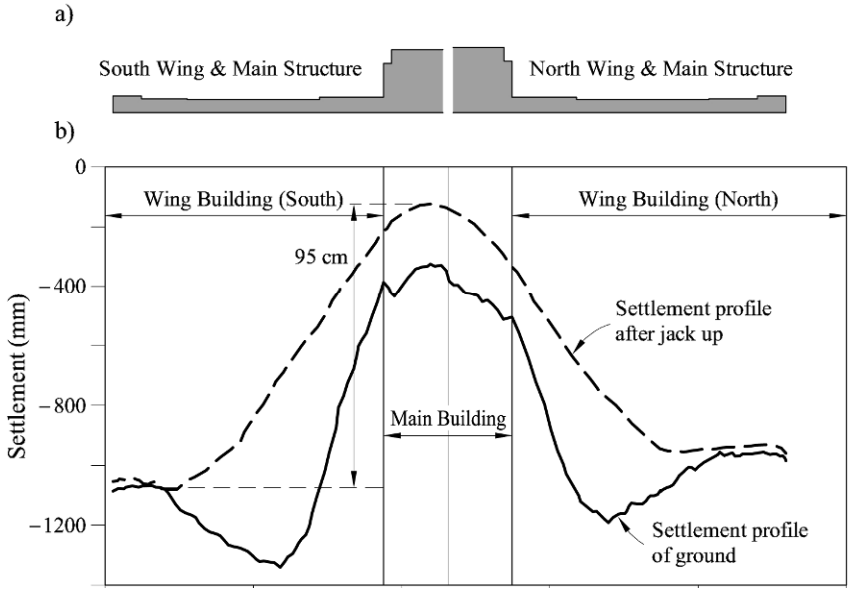

Figure 2.14 The passenger terminal building (after Akai and Tanaka, 2005: © 2005, IOS Press, used with permission): (a) outline; (b) settlement profiles along the longitudinal line.

2.5 Lessons Learned

2.5.1 High level of indeterminacy

The major problem with large-scale land reclamation projects is that it is almost impossible to provide an accurate prediction of the rates of settlement based solely on the results of site investigation and laboratory consolidation tests. The major reasons for that are large spatial variability of soil properties and drainage geometry and the fact that laboratory tests often produce values of the coefficients of consolidation and secondary compression within two orders of magnitude (i.e. 10^2) from the field values – with the field exhibiting more pervious behaviour. Therefore, such estimates can only be used as initial conditions for design.

2.5.2 Immediate settlements

Immediate settlements in saturated clay layers in a one-dimensional problem

should be zero. In reality, however, there are always some immediate settlements caused by the three-dimensionality of the real problem, which involves non-negligible lateral and, hence, vertical strains. In the layered sand-clay systems, however, some immediate settlements occur even in a one-dimensional problem. This is due to the compressibility of the sand layers, where pores are sufficiently large to allow for almost immediate dissipation of pore water pressures.

2.5.3 Limited drainage

The rate of consolidation is determined to a large extent by the length of the drainage path. Conventionally, a sand layer between two clay layers is considered to work as a drain. There are cases, however, where some of the sand layers appear to be lenses, entirely enclosed within a clay layer. It is important to observe dissipation of the pore water pressures in sand layers during the construction, in order to determine their draining ability.

2.5.4 Secondary compression

It is important to remember that the consolidation process is not the only one controlling the rate of the settlements in clay. Even when the excess pore water pressure has completely dissipated, different physical phenomena cause continued settlement. While this secondary compression is present from the beginning of the consolidation process, towards the end of primary consolidation its contribution becomes more visible. The secondary compression may produce a significant increase in settlements long after the primary consolidation is over.

2.5.5 The observational method

Because of the high level of indeterminacy in such projects, the observational method should be adopted in design and construction. In this method, the design is left flexible to accommodate changes as construction proceeds. The changes should be based on the continuous monitoring of significant field parameters and on inverse analysis of the field measurements. This back calculation allows for model parameters to be updated using real field data and then utilized for the next stages of design.

References

Akai, K., Nakaseko, K., Matsui, T., Kamon, K., Sugano, M., Tanaka, Y. and Suwa, S. (1995) Geotechnical and geological studies on seabed Osaka Bay. *Proceedings of the 11th European Conference on Soil Mechanics and Foundation Engineering* 8, 8.1 – 8.6.

Akai, K. and Tanaka, Y. (1999) Settlement behaviour of an off-shore airport KIA. *Geotechnical Engineering for Transportation Infrastructure*, 1041–1046.

Akai, K. and Tanaka, Y. (2005) Ex-Post-Facto estimate of performance at the offshore reclamation of airport Osaka/KIA. *Proceedings of the 16th International Conference on Soil Mechanics and Geotechnical Engineering* 2, 1011 – 1014.

Endo, H., Oikawa, K., Komatsu, A. and Kobayashi, M. (1991) Settlement of diluvial clay layers caused by a large scale man-made island. *Geo-Coast 91'*, 177 – 182.

Handy, R.L. (2002) First-order rate equations in geotechnical engineering. *ASCE Journal of Geotechnical and Geoenvironmental Engineering* 128 (5), 416 – 425.

KALD (2009) Kansai Airport Land Development Company, Website: www.kald.co.jp

Matsui, T., Oda, K. and Tabata, T. (2003) Structures on and within man-made deposits – Kansai Airport. *Proceedings of the 13th European Conference on Soil Mechanics and Geotechnical Engineering* 3, 315 – 328.

Mesri, G. and Varhanabhuti, B. (2005) Secondary compression. *ASCE Journal of Geotechnical and Geoenvironmental Engineering* 131 (3), 398 – 401.

Terzaghi, K. (1943) *Theoretical Soil Mechanics*, John Wiley and Sons, New York.

http://www.springer.com/978-90-481-3530-1

Geomechanics of Failures

Puzrin, A.M.; Alonso, E.E.; Pinyol, N.M.

2010, VIII, 245 p., Hardcover
ISBN: 978-90-481-3530-1